RESEARCH ARTICLE | JULY 17 2023

Performance scaling with an applied magnetic field in indirect-drive inertial confinement fusion implosions FREE

Special Collection: Papers from the 64th Annual Meeting of the APS Division of Plasma Physics

H. Sio; J. D. Moody; B. B. Pollock; D. J. Strozzi; D. D.-M. Ho; C. A. Walsh; G. E. Kemp; B. Lahmann; S. O. Kucheyev; B. Kozioziemski; E. G. Carroll; J. Kroll; D. K. Yanagisawa; J. Angus; B. Bachmann; A. A. Baker; L. B. Bayu Aji; S. D. Bhandarkar; J. D. Bude; L. Divol; A. M. Engwall; B. Ferguson; J. Fry; L. Hagler; E. Hartouni; M. C. Herrmann; W. Hsing; D. M. Holunga; J. Javedani; A. Johnson; S. Khan; D. Kalantar; T. Kohut; B. G. Logan; N. Masters; A. Nikroo; N. Izumi; N. Orsi; K. Piston; C. Provencher; A. Rowe; J. Sater; S. J. Shin; K. Skulina; W. A. Stygar; V. Tang; S. E. Winters; G. Zimmerman; J. P. Chittenden; B. Appelbe; A. Boxall; A. Crilly; S. O'Neill; D. Barnak; J. Davies; J. Peebles; J. H. Bae; K. Clark; M. Havre; M. Mauldin; M. Ratledge; S. Vonhof; P. Adrian; B. Reichelt; S. Fujioka; M. Fraenkel

Physics of Plasmas 30, 072709 (2023)
https://doi.org/10.1063/5.0150441

Physics of Plasmas ARTICLE pubs.aip.org/aip/pop

Performance scaling with an applied magnetic field in indirect-drive inertial confinement fusion implosions

Cite as: Phys. Plasmas **30**, 072709 (2023); doi: 10.1063/5.0150441
Submitted: 14 March 2023 · Accepted: 27 June 2023 ·
Published Online: 17 July 2023

View Online Export Citation CrossMark

H. Sio,[1,a),b)] J. D. Moody,[1] B. B. Pollock,[1] D. J. Strozzi,[1] D. D.-M. Ho,[1] C. A. Walsh,[1] G. E. Kemp,[1] B. Lahmann,[1] S. O. Kucheyev,[1] B. Kozioziemski,[1] E. G. Carroll,[1] J. Kroll,[1] D. K. Yanagisawa,[1] J. Angus,[1] B. Bachmann,[1] A. A. Baker,[1] L. B. Bayu Aji,[1] S. D. Bhandarkar,[1] J. D. Bude,[1] L. Divol,[1] A. M. Engwall,[1] B. Ferguson,[1] J. Fry,[1] L. Hagler,[1] E. Hartouni,[1] M. C. Herrmann,[1] W. Hsing,[1] D. M. Holunga,[1] J. Javedani,[1] A. Johnson,[1] S. Khan,[1] D. Kalantar,[1] T. Kohut,[1] B. G. Logan,[1] N. Masters,[1] A. Nikroo,[1] N. Izumi,[1] N. Orsi,[1] K. Piston,[1] C. Provencher,[1] A. Rowe,[1] J. Sater,[1] S. J. Shin,[1] K. Skulina,[1] W. A. Stygar,[1] V. Tang,[1] S. E. Winters,[1] G. Zimmerman,[1] J. P. Chittenden,[2] B. Appelbe,[2] A. Boxall,[2] A. Crilly,[2] S. O'Neill,[2] D. Barnak,[3] J. Davies,[3] J. Peebles,[3] J. H. Bae,[4] K. Clark,[4] M. Havre,[4] M. Mauldin,[4] M. Ratledge,[4] S. Vonhof,[4] P. Adrian,[5] B. Reichelt,[5] S. Fujioka,[6] and M. Fraenkel[7]

AFFILIATIONS

[1]Lawrence Livermore National Laboratory, Livermore, California 94550, USA
[2]Centre for Inertial Fusion Studies, The Blackett Laboratory, Imperial College, London SW7 2AZ, United Kingdom
[3]Laboratory for Laser Energetics, University of Rochester, New York 14623, USA
[4]General Atomics, San Diego, California 92121, USA
[5]Massachusetts Institute of Technology, Cambridge, Massachusetts 02139, USA
[6]Institute for Laser Engineering, Osaka University, 2-6 Yamada-Oka, Suita, Osaka 565-0871, Japan
[7]Plasma Physics Department, Soreq NRC, Yavne 81800, Israel

Note: This paper is part of the Special Collection: Papers from the 64th Annual Meeting of the APS Division of Plasma Physics.
Note: Paper NI2 6, Bull. Am. Phys. Soc. **67** (2022).
[a)]Invited speaker.
[b)]**Author to whom correspondence should be addressed:** sio1@llnl.gov

ABSTRACT

Magnetizing a cryogenic deuterium–tritium (DT)-layered inertial confinement fusion (ICF) implosion can improve performance by reducing thermal conduction and improving DT-alpha confinement in the hot spot. A room-temperature, magnetized indirect-drive ICF platform at the National Ignition Facility has been developed, using a high-Z, high-resistivity $AuTa_4$ alloy as the *hohlraum* wall material. Experiments show a 2.5× increase in deuterium–deuterium (DD) neutron yield and a 0.8-keV increase in hot-spot temperature with the application of a 12-T B-field. For an initial 26-T B-field, we observed a 2.9× yield increase and a 1.1-keV temperature increase, with the inferred burn-averaged B-field in the compressed hot spot estimated to be 7.1 ± 1.8 kT using measured primary DD-n and secondary DT-n neutron yields.

I. INTRODUCTION

In an inertial confinement fusion (ICF) implosion,[1] laser or x-ray drive is used to implode a capsule filled with deuterium–tritium fuel. Specifically, indirect-drive ICF experiments use a high-Z cavity (*hohlraum*) to convert laser energy to x-ray drive,[2,3] which, in turn, ablates and compresses the capsule. In the capsule during peak compression, fusion energy gain from deuterium–tritium (DT)-α energy deposition into the hot spot is balanced against energy loss from the hot spot through radiative loss and thermal conduction. Fusion ignition, as recently demonstrated[4–6] in indirect-drive ICF implosions at the National Ignition Facility (NIF),[7] is achieved when fusion heating power in the plasma exceeds all physical processes that cool the plasma. As a critical milestone toward the development of inertial fusion energy, a target gain greater than one, defined as when the fusion energy produced in the target exceeds the laser energy delivered to the target, has also been experimentally demonstrated.[8]

An externally applied magnetic field has been proposed as a promising mechanism to further improve an already high-performing ICF implosion by reducing electron thermal conduction and magnetically confining the DT-α in the hot spot.[9,10] These two benefits are respectively realized when the electron gyroradius is smaller than the electron mean free path (electron Hall parameter exceeding unity), and when the DT-α gyroradius is smaller than the hot-spot radius. Enhanced fusion yield and temperature have been reported in cylindrical magnetized liner inertial fusion implosions[11–13] and magnetized direct-drive ICF implosions.[14] Recent experiments at the NIF have also demonstrated performance enhancement from an applied B-field in room-temperature ("warm") indirect-drive implosions.[15] This work provides additional details on these implosion experiments and also describes new results on yield and temperature enhancements at intermediate B-field. The warm magnetized experiments here demonstrated robust yield and temperature enhancements even with a modest 12-T initial B-field, potentially relaxing the initial B-field requirement in future cryogenic DT-layered platforms. These warm magnetized experiments provide an important physics demonstration that magnetizing an implosion led to tangible performance improvements, and no deleterious effects were observed due to the introduction of the magnetic field. We also discuss experimental results on the OMEGA[16] laser facility characterizing the $AuTa_4$ *hohlraum* wall material used in these indirect-drive experiments.

Following the introduction section, Sec. II discusses experiments characterizing the new *hohlraum* wall material needed to field an indirect-drive magnetized target. Section III provides an overview of the experiment setup at NIF and the stagnated hot spot shape-tuning efforts at the onset of the campaign. Section IV describes yield and temperature enhancement as a function of initial B-field and comparison with simulations, while Sec. V provides an estimate of the burn-averaged B-field in the compressed hot spot. Section VI summarizes and discusses the path forward toward a magnetized cryogenic DT-layered implosion at NIF.

II. DEVELOPMENT AND TESTING OF NEW *HOHLRAUM* WALL MATERIALS

The presence of strong currents and magnetic fields drive new physics and engineering constraints in the *hohlraum* design. Magnetic field is applied to the capsule by driving large currents through copper wires wrapped around the *hohlraum*, so a highly-conductive *hohlraum* [such as one typically made from Au or depleted uranium (DU)] presents several physics issues. At room temperature, electrical resistivities of Au and U are ~2 and ~30 $\mu\Omega$ cm,[17] respectively. Eddy currents are induced by the external B-field in the *hohlraum* wall, increasing the time needed for the B-field to diffuse through the wall and into the capsule. These eddy currents also drive a temperature increase in the *hohlraum* wall (which radiates and preheats the capsule) and create inward motion of the *hohlraum* wall prior to the arrival of the lasers. These problems are exacerbated at cryogenic temperature ($T \approx 20$ K) where electrical resistivity is significantly

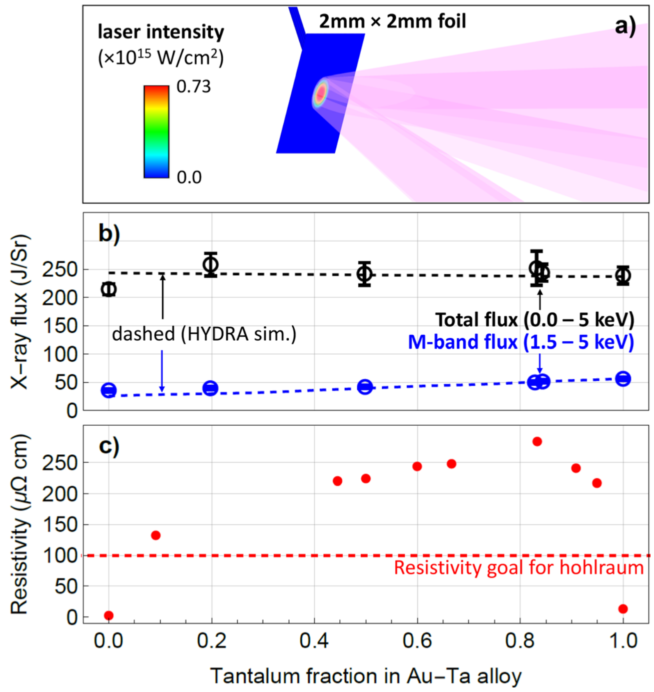

FIG. 1. (a) Experimental configuration for measurement of Au–Ta alloy x-ray flux on OMEGA. (b) The measured total flux (black) and M-band (>1.5 keV) flux (blue) as a function of Ta fraction in the Au–Ta alloy, with trends from HYDRA simulations shown as dashed lines. (c) The measured electrical resistivity as a function of tantalum fraction in the Au–Ta samples.

lower than room-temperature values due to reduced phonon scattering. These concerns[18] drive the need for a high-resistivity (>100 $\mu\Omega\cdot$ cm), high-Z *hohlraum* material with similar x-ray performance as Au.

Such a *hohlraum* material was developed using an alloy of gold and tantalum (specifically, $AuTa_4$). The first iteration of Au-Ta alloy tested at the OMEGA experiment described below is made using direct current magnetron co-sputtering on planar substrates.[19] Later, films deposited onto a spherical-cylindrical substrate (for *hohlraums* used at the NIF) used either alloyed-target direct current magnetron sputtering[20,21] or pulsed plasma deposition.[22–24] The high resistivity of the sputter-deposited Au-Ta films is caused by the peculiarities of electronic transport in the non-equilibrium microstructure with either an amorphous or beta-Ta dominated phase.

As examples, the magnetic diffusion time scales for a 15-μm-thick cylinder 2.7 mm in radius are 1.3 μs for Au vs 15 ns for $AuTa_4$.[18] This magnetic diffusion time estimate ($\tau_0 = \mu_0 \sigma \delta R/2$, where μ_0, σ, δ, and R are the permeability of free space, electrical conductivity, cylinder thickness, and cylinder radius, respectively) does not take into account the temperature-dependent resistivity due to Ohmic heating from eddy current dissipation, which is discussed in more details in Moody *et al.*[18]

While we may be concerned that introducing a lower-Z element such as Ta may lower the overall x-ray efficiency as compared to pure Au, this is partially mitigated by the "cocktail effect,"[2,25–28] the

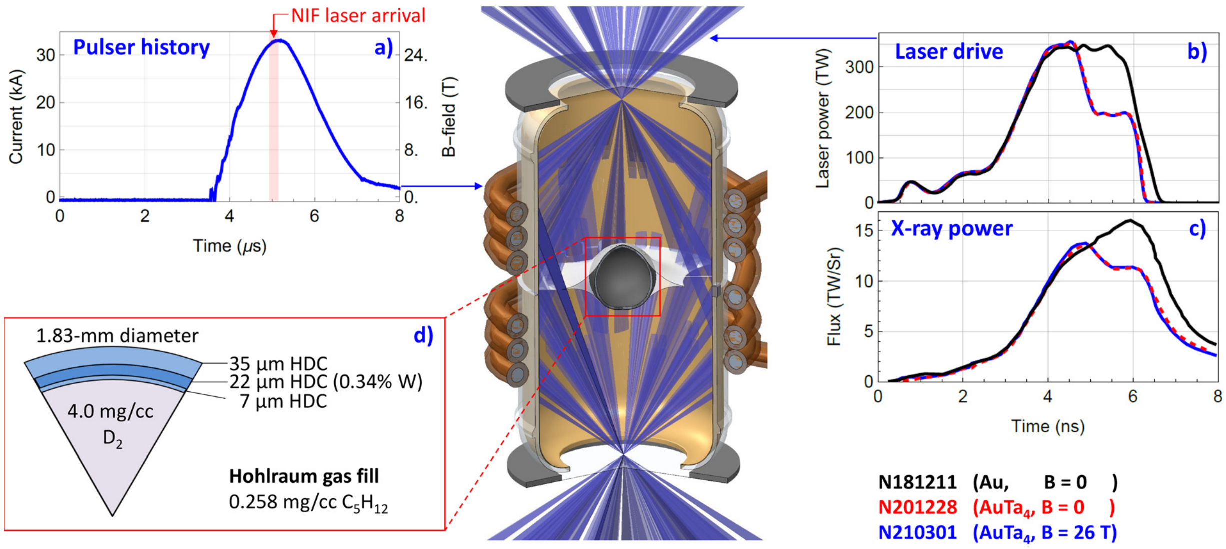

FIG. 2. Overview of the magnetized indirect-drive implosion platform, showing (a) the pulser current history, (b) laser drive, (c) measured total x-ray power, and (d) capsule design. For (b) and (c), N210301 (blue) and N201228 (red) are two experiments using the new $AuTa_4$ hohlraum, with and without an applied B-field, respectively. N181211 is a reference implosion from a different campaign using an Au *hohlraum* and similar laser drive.

phenomenon of higher-Rosseland mean opacity of certain alloy combinations as compared to individual components alone by filling in the low-opacity region of one material with the high-opacity region of another material. The overall higher opacity leads to reduced radiation loss to the wall, higher albedo, and higher coupling of the *hohlraum* radiation to the capsule implosion.

Prior to the efforts needed to field this Au-Ta alloy as a *hohlraum* target at NIF, we first performed an experiment at the 60-beam OMEGA laser facility[16] with flat-foil targets made from this Au-Ta alloy with varying Ta fraction. The foil target is irradiated by a set of five 351-nm beams at 21.4° angle of incidence relative to the foil surface normal using a 1-ns duration uniform pulse shape with a total peak power of 1.8 TW. The total intensity on target is 7×10^{14} W/cm^2, comparable to the intensity reached by a NIF laser quad.[29] The laser drive uses smoothing by spectral dispersion and phase plates with a 574-μm-diameter (1/e) spot size with a super-Gaussian order of 5.1.

X-ray emission measurements are made using DANTE,[30,31] a 15-channel x-ray diode system with K-edge and L-edge filters. Careful selection of filters creates combined channel responses that have high sensitivity in the regions below the filter absorption edges. An absolute soft x-ray flux is obtained by analyzing the recorded diode voltages with the channel x-ray responses using a genetic algorithm[32] to reconstruct a probabilistic spectral intensity distribution.

Figure 1 shows the total x-ray flux, M-band flux (x-ray flux above 1.5 keV), and electrical resistivity of Au–Ta alloy as a function of Ta fraction from pure gold to pure tantalum. We observe that the measured x-ray flux trend is relatively flat (consistent with Dewald *et al.*[2] at ICF-relevant intensities), and there is an increase in M-band fraction as the Ta fraction increases. Because the Au-Ta alloy resistivity peaks near 80% Ta, $AuTa_4$ was chosen to be the new *hohlraum* material for the magnetized indirect-drive experiment at the NIF, with this set of data providing the first experimental evidence that a high-resistivity Au-Ta alloy has similar x-ray performance as Au.

III. INDIRECT-DRIVE IMPLOSIONS AT THE NATIONAL IGNITION FACILITY

Figure 2 presents an overview of the magnetized warm indirect-drive platform at the NIF. The magnetized target is a millimeter-scale capsule in the center of a high-Z *hohlraum*. High voltage is pulsed through copper wires wrapped outside the *hohlraum*, driving up to a peak current of 34 kA over 5 μs. The magnetic field (to a peak of 26 T at the capsule) induced by the currents diffuses through the *hohlraum* wall into the capsule and is later compressed and amplified when the capsule implodes to a much smaller radius.

The $AuTa_4$ *hohlraum* is 5.4 mm in diameter, with 3.4-mm diameter laser entrance holes, and filled with 0.258 mg/cm^3 of neopentane (C_5H_{12}). The capsule is 1.83 mm in diameter, with a high-density-carbon (HDC) shell 64-μm thick, and an intermediate layer doped with 0.34 at. % W. The capsule is held in place by 40-nm-thick membranes (tents) and filled with 4 mg/cm^3 of deuterium fuel through a 10-μm-diameter fill tube.

In total, 192 laser beams are directed toward the inside of the *hohlraum*, converting laser light at 351-nm (3ω) wavelength to thermal x rays that ablate and implode the capsule target. NIF laser beams are smoothed by spectral dispersion, polarization smoothing, and continuous phase plates. The target and laser design (when unmagnetized) are very similar to the high-adiabat BigFoot campaign[33–35] [with N181211 as an example in Figs. 2(c) and 2(d)]. One notable change in the laser drive is that power is reduced at late time (after 5 ns), as this initial set of magnetized indirect-drive experiments are limited in laser power due to pulser pre-fire concern. A pulser pre-fire mitigation system is being implemented on the NIF, which will enable full use of NIF laser power in magnetized implosions in the future.

The laser drive similarity to the previous BigFoot campaign which used an Au *hohlraum* also provides an opportunity to directly compare x-ray performance of Au vs $AuTa_4$ *hohlraums* [Fig. 2(c)]. The x-ray flux is measured with the NIF DANTE system[36] with increased dynamic range for radiation temperature up to 1 keV and flux between 10^{10}–10^{14} W/cm^2. Up until 5 ns, when the laser drives begin to diverge [Fig. 2(b)], the measured DANTE x-ray flux histories are very similar between the experiment using an Au *hohlraum* (N181211) and the experiment using an $AuTa_4$ *hohlraum* (N201228). This is consistent with the experimental results from driven flat-foil targets discussed in Sec. II. In addition, the measured DANTE x-ray flux histories are very similar between $AuTa_4$ experiments without an applied B-field (N201228) and with a 26-T applied B-field (N210301). These measurements demonstrate that the *hohlraum* x-ray drive is unaffected by the applied magnetic field and is effectively the same between Au and $AuTa_4$ *hohlraums*.

The 192 NIF laser beams are grouped into 48 quads, with 4, 4, 8, and 8 quads at 23.5°, 30°, 44.5°, and 50°, respectively, relative to the *hohlraum* axis on each hemisphere of the target chamber. Backscatter out of the *hohlraum* is measured using a full-aperture-backscatter system (FABS) and near-backscatter imager (NBI) on one 30° quad and one 50° quad.[37] The 23.5° and 30° beams are referred to as the inner beams, while the 44.5° and 50° beams are the outer beams. This distinction is important because the inner and outer beams are incident on different locations on the *hohlraum* along the *hohlraum* axis (see Fig. 3), and the relative powers between the inner and outer beams are used to control implosion shape. Cone fraction (CF) in this manuscript refers to the peak inner-beam power divided by the peak total power. The nominal NIF cone fraction is 33%, when inner and outer beams are at full power.

The first integrated warm magnetized indirect-drive experiment at 26 T (N210301) used a cone fraction of 27%, which produced a significantly prolate hot spot [Fig. 3(b)]. Adjusting the cone fraction to 23% in a later magnetized experiment (N210607) successfully tuned the hot-spot shape to round, and a 23% cone fraction is used in all subsequent experiments. The difference in inner and outer beam powers for 27% vs 23% cone fraction is shown in Fig. 3(c).

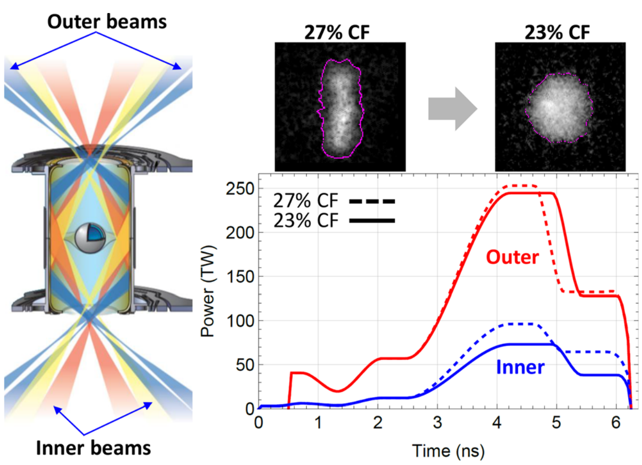

FIG. 3. Outer and inner beam laser pulse shapes and implosion x-ray shape at stagnation from the equator, for two magnetized (B = 26 T) indirect-drive implosions with 27% cone fraction (N210301) and 23% cone fraction (N210607).

IV. B-FIELD SCALING AND COMPARISON WITH SIMULATIONS

This section discusses the scaling of neutron yield and ion temperature as a function of applied B-field in these warm, indirect-drive magnetized implosions, focusing on four experiments which are summarized in Fig. 4. When evaluating yield and ion temperature amplifications, we compare the values from magnetized experiments to the no-B baseline experiments. The first important observation from Figs. 4(b) and 4(c) is that with a 26-T applied B-field, we observed a 2.9× increase in deuterium–deuterium (DD) yield and a 1.1-keV

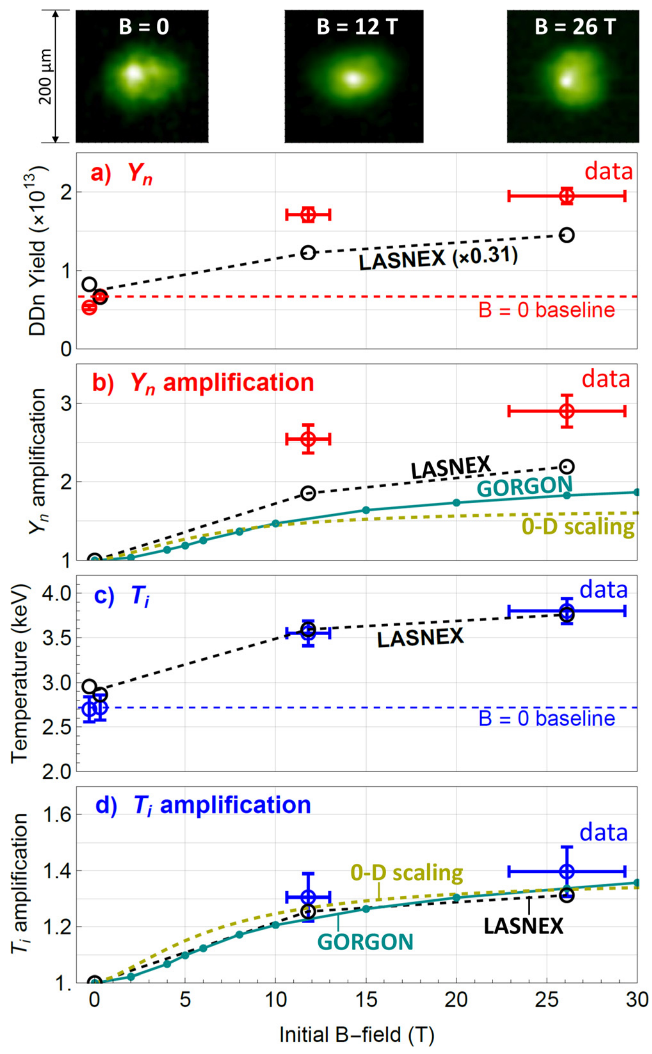

FIG. 4. (a) DD neutron yield, (b) DD neutron yield amplification, (c) DD ion temperature, and (d) DD ion temperature amplification as a function of initial B-field in four warm, magnetized indirect-drive experiments. Measured yields and temperatures are shown in red and blue, respectively. Post-shot LASNEX simulated yields and temperatures are shown in black open circles (with trend lines to guide the eyes), and expected amplification scaling from GORGON are shown in teal. Analytic 0D scaling[40] is shown in yellow. A tabular summary is provided in Table I. Equatorial x-ray images at bang time for implosions with different initial B-field are shown on top.

increase in DD ion temperature. Equally important is that even at an intermediate 12-T B-field, we observed a 2.5× increase in DD yield and a 0.8-keV increase in DD ion temperature, providing direct experimental evidence that even a modest B-field can lead to significant improvement in implosion performance.

These experimental values are compared against post-shot simulations using the 2D radiation-magnetohydrodynamic (MHD) code LASNEX,[38,39] which includes the MHD processes of Nernst advection, resistive diffusion, magnetized thermal conduction, Righi–Leduc heat flow, Biermann-battery-generated fields, and the Lorentz force. These post-shot simulations used a laser power multiplier and a cone-fraction multiplier to match the measured capsule peak-emission time (bang time) and implosion shape (P_2 Legendre moment). Overall, simulated ion temperatures (absolute magnitude and scaling with B-field) are in good agreement with data. The simulated DD yields are ∼2×–3× higher, and the simulated yield amplification as a function of B-field is lower than what is experimentally observed. Both diffuse and localized mixes (bright x-ray emission spot on the x-ray images in Fig. 4 (top) corresponding to the fill tube) are likely yield degradation mechanisms.

Capsule-only simulations at different magnetic fields are also performed using the 3D Eulerian MHD code GORGON.[41,42] The expected yield and temperature amplifications as a function of B-field are plotted in Figs. 4(b) and 4(d), respectively. We also compare these simulation values to analytic scaling[40] of yield and temperature in a magnetized hot spot, with the temperature scaling as $\kappa_{eff}^{-2/7}$, assuming a 0D plasma and Spitzer–Härm thermal conductivity.[43] Here, $\kappa_{eff} = 1/3 + (2/3)\kappa_{\|}/\kappa_{\perp}$ is the effective thermal conductivity and a sum of the thermal conductivities parallel ($\kappa_{\|}$) and perpendicular ($\kappa_{\perp}$) to the magnetic field direction. Inputs to the yield scaling[40] are the unmagnetized hot-spot temperature (using measured values) and averaged electron Hall parameter ($\omega_e\tau_e$) (from LASNEX). At 26-T initial B-field, the simulated $\omega_e\tau_e$ in the magnetized hot spot during stagnation is ∼4, corresponding to an effective thermal conductivity κ_{eff} of 0.37 (as compared to 1, without a magnetic field).

DD neutron yield and temperature are measured using neutron time of flight (nTOF)[44] detectors. The arrival time of a fusion neutron at the detector is related to the energy of the neutron. The burn-averaged DD temperature is inferred from the width of the neutron energy spectrum, specifically, the component from thermal Doppler broadening. However, non-thermal motions in the plasma due to radial or turbulent flows can also lead to additional broadening, contributing to a higher apparent DD temperature.[45,46] To address this, emission-averaged electron temperature measurements [Fig. 5(b)] show independent confirmation of temperature increase in the hot spot with the application of an external B-field, ruling out the possibility that the increase in DD ion temperature may have been due to increased fluid motions. The electron temperature is inferred from the x-ray continuum emission penumbral[47] images of the stagnated hot spot behind different x-ray filters.[48,49] Because the emission-averaged x-rays and burn-averaged DD neutrons probe different regions of the hot spot and because the emission-averaged x-ray temperature is filtration-dependent, we do not expect the x-ray and neutron temperatures to be the same.

V. COMPRESSED B-FIELD IN THE HOT SPOT

We also estimate the burn-averaged compressed B-field in the hot spot using the measured ratio of the secondary DT neutrons to primary DD neutrons (Y_{DT}/Y_{DD}). In a deuterium plasma, we refer to the 2.45-MeV fusion DD-n[50] as the primary DD neutron

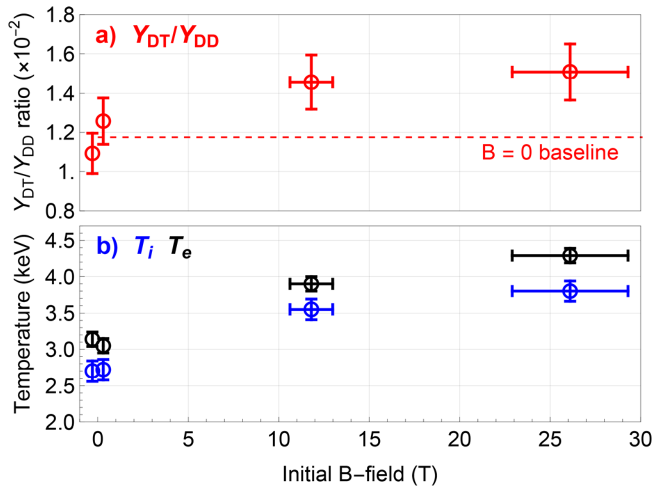

FIG. 5. (a) Secondary DTn to primary DDn yield ratio (red) and (b) burn-averaged DD temperature measured using neutron time of flight detectors (blue) and emission-averaged electron temperature measured using x-ray penumbral images (black) as a function of initial B-field.

$$\mathrm{D} + \mathrm{D} \rightarrow \mathrm{n}(2.45\,\mathrm{MeV}) + {}^3\mathrm{He}(0.82\,\mathrm{MeV}). \quad (1)$$

The second branch of the DD reaction produces a 1.01-MeV DD-t, and as this DD-t transits the hot spot, it has a probability to undergo a second fusion reaction with a background deuteron, generating a fusion DT-n, referred to here as a secondary DT neutron,

$$\mathrm{D} + \mathrm{D} \rightarrow T(1.01\,\mathrm{MeV}) + \mathrm{p}(3.02\,\mathrm{MeV}), \quad (2)$$

$$\mathrm{D} + \mathrm{T}(\leq 1.01\,\mathrm{MeV}) \rightarrow \mathrm{n}(11.9 - 17.2\,\mathrm{MeV}) + \alpha(6.7 - 1.4\,\mathrm{MeV}). \quad (3)$$

As the areal density (ρR) of the hot spot increases, the DD-t lose more energy and have a higher fusion probability, increasing the secondary yield ratio Y_{DT}/Y_{DD}. As the secondary yield ratio is sensitive to plasma parameters that affect stopping power, it has been used estimate fuel areal density[51] and/or mix.[52] In the presence of a strong magnetic field, these DD-t can also be magnetically confined, increasing their path lengths, energy loss, and secondary DT fusion probability in the hot spot. This method of using the secondary yield ratio to infer fuel magnetization has been developed for cylindrical ICF implosions[53,54] and later extended to spherical ICF implosions.[55]

Figure 6 shows the secondary yield ratio Y_{DT}/Y_{DD} as a function of B-field and electron temperature as calculated using a static Monte Carlo model,[55] assuming uniform density and temperature profiles with an areal density of 60 mg/cm^2 (to match the measured Y_{DT}/Y_{DD} in the no-B experiment). As expected, Y_{DT}/Y_{DD} increases when temperature decreases (increasing the plasma stopping power) and when the B-field increases (better confining the DD-t).

Figure 5(a) shows the Y_{DT}/Y_{DD} as a function of initial B-field, and we observed a modest increase in the measured Y_{DT}/Y_{DD} in the magnetized implosions as compared to the unmagnetized implosions. As the measured electron temperature in the hot spot increases with

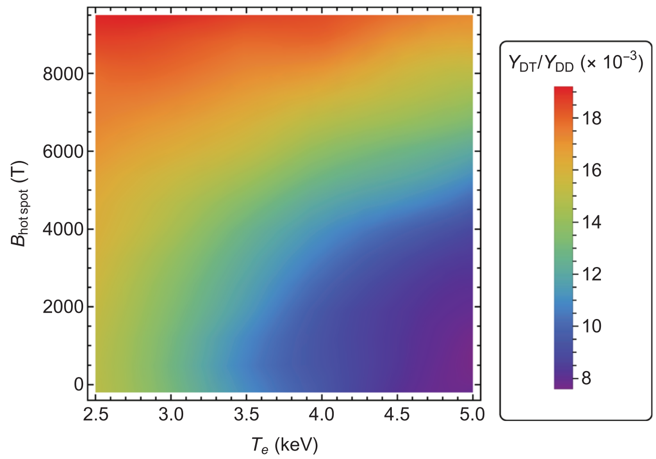

FIG. 6. The secondary yield ratio Y_{DT}/Y_{DD} as a function of B-field and electron temperature as calculated using a static Monte Carlo model[55] for a fuel ρR

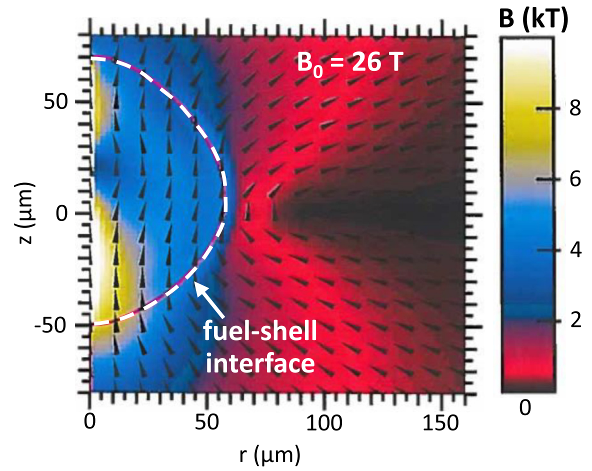

FIG. 7. B-field vector map from a LASNEX simulation of a magnetized implosion with an initial B-field of 26 T (N210607) near peak stagnation (convergence ∼ 15). The white-dashed line is the fuel–shell interface, and the color scale represents the B-field magnitude.

an applied B-field, which would lower Y_{DT}/Y_{DD} because of reduced stopping power in the hot spot, a corresponding increase in the hot-spot B-field is needed to explain the increase in Y_{DT}/Y_{DD}. Using the static Monte Carlo model described above, for N220912 ($B_0 = 12$ T) and N210607 ($B_0 = 26$ T), the estimated B-fields are 6.3 ± 1.6 and 7.1 ± 1.8 kT, respectively, reflecting uncertainties in the measured temperature, implosion size, and Y_{DT}/Y_{DD}.

Assuming no magnetic flux loss and using the measured capsule convergence from hot-spot x-ray imaging (B-field scales as the square of the convergence ratio), the estimated compressed B-field in the hot spot for N220912 ($B_0 = 12$ T) and N210607 ($B_0 = 26$ T) are 2.7 and 6.6 kT, respectively. These values are also consistent with the B-field magnitudes in 2-D LASNEX magnetohydrodynamic simulations near peak stagnation (Fig. 7), showing average B-field magnitude in the hot spot of ∼4–6 kT for a magnetized implosion with an initial 26 B-field. We nominally expect a linear relationship between the initial applied B-field and the final compressed B-field in the hot spot, so the relatively high estimated B-field for N220912 ($B_0 = 12$ T) is unexpected. An additional implosion experiment at $B_0 = 12$ T (N220110), which is nominally identical to N220912 except without a *hohlraum* gas fill due to target leakage, measured very similar hot-spot size, temperature, and Y_{DT}/Y_{DD}, so this discrepancy does not appear to be related to random experimental uncertainties.

To magnetize electrons we require the electron Hall parameter $\omega_e\tau_e = 1.91 \times 10^{21}\, B[T]\, (T_e[keV])^{3/2}/(n_e[cm^{-3}]\, \ln \Lambda)$ to be greater than unity, where B, T_e, n_e, and $\ln \Lambda$ are the B-field, electron temperature, electron number density, and the Coulomb Logarithm, respectively. The effect of electron magnetization can be indirectly observed through increases in yield and temperature, and requires a modest B-field of >1–2 kT. In contrast, magnetic confinement of DD-t in the plasma requires the ratio of plasma radius to DD-t gyroradius $R_{fuel}/R_{gyro,t} = 5.4 \times 10^{-6}\, B[T]\, R[\mu m]$ to exceed unity,[55] requiring > 4 kT for a 50-μm-radius hot spot. That is, for typical warm indirect-drive plasma conditions, observing an increase in the secondary yield ratio Y_{DT}/Y_{DD} with the application of an external B-field (see Table I) is a more stringent experimental confirmation that the fuel is magnetized as compared to increases in temperature and yield due to magnetic thermal insulation.

VI. DISCUSSION

The yield and ion temperature increases in magnetized warm indirect-drive implosions observed in this work pave the path forward to fielding a magnetized cryogenic DT-layered target on NIF. The benefits of thermal conduction suppression from an applied B-field is expected to be the same in warm and cryogenic implosions,[40] and in a burning hot spot, the compressed B-field has the additional benefit of magnetically confining the DT-α. Simulation of an igniting cryogenic DT-layered implosion (N210808)[4–6] with a 40-T initial B-field shows a 2× increase in yield and a 40% increase in temperature.[56] This example magnetized cryogenic DT-layered implosion has an peak mass-weighted hot-spot temperature of 14 keV, $\rho R \sim 0.45$ g/cm^2, a convergence ratio of 22.8, and a volume-averaged B-field ∼24 kT.

The warm magnetized experiments here demonstrated robust yield and temperature enhancements even with a modest initial 12-T B-field, potentially relaxing the initial B-field requirement in future cryogenic DT-layered platforms. These warm magnetized experiments provide an important physics demonstration that an external magnetic field (1) can be applied to an indirect-drive target through the high-Z *hohlraum* wall, 2) provided tangible implosion performance improvements, and 3) did not lead to observable deleterious effects in the capsule or in the *hohlraum*. Future warm magnetized experiments will also study the potential benefits of an applied B-field in suppressing mix.[57] While the positive results in these warm, lower-convergence implosions have yet to be demonstrated in DT-layered, higher-convergence implosions, they nonetheless serve an important role in benchmarking MHD codes and models and as a platform for assessing new magnetized implosion designs.

In summary, a warm, magnetized indirect-drive ICF platform at the National Ignition Facility has been developed, including a high-Z, high-resistivity $AuTa_4$ alloy as the *hohlraum* wall material. Applying an initial 12-T B-field to a ∼900-kJ ICF implosion leads to a 2.5× increase in yield and 0.8-keV increase in hot-spot temperature. For an

TABLE I. Implosion data summary and simulated quantities from post-shot LASNEX simulations. All experiments used nominally identical capsules (Fig. 2). All experiments listed except N210301 used nominal 23% laser cone fraction and D_2 capsule gas fill. Typical measurement uncertainties are as follows: $\pm 3\,\mu$m for P_0 and P_2, $\pm 5\%$ for Y_{DD}, $\pm 10\%$ for Y_{DT}, ± 0.15 keV for $T_{i,DD}$ and T_e, and ± 0.05 ns for bang time. For the convergence ratio R_0/P_0, R_0 is the initial capsule radius and P_0 is the x-ray P_0 at stagnation. Yield (Y) refers to neutron yield. No equatorial x-ray image was obtained on N210717.

	Unit	N210301	N210717	N210912	N220110	N220912	N210607
$B_{initial}$	T	26.1	0	0	11.8	11.8	26.1
Laser energy	kJ	926	875	840	898	874	883
Cone fraction (peak)		0.27	0.23	0.22	0.23	0.23	0.23
Capsule gas fill		30% D–70% ^{4}He	D_2	D_2	D_2	D_2	D_2
Capsule gas fill density	mg/cm^3	5.1	3.9	4.0	4.0	4.0	4.0
hohlraum gas fill		C_5H_{12}	C_5H_{12}	C_5H_{12}	D_2	C_5H_{12}	C_5H_{12}
hohlraum gas fill density	mg/cm^3	0.26	0.26	0.26	0.01	0.26	0.26
x-ray P_0	μm	51	...	59	53	56	54
x-ray P_2	μm	32	...	−10	13	−9	3
Convergence ratio (R_0/P_0)		16.6	...	15.3	16.1	15.2	15.6
Y_{DD}		5.0×10^{11}	5.3×10^{12}	6.7×10^{12}	2.2×10^{13}	1.7×10^{13}	2.0×10^{13}
Y_{DD} (LASNEX)		1.1×10^{12}	2.6×10^{13}	2.1×10^{13}	...	3.9×10^{13}	4.6×10^{13}
Y_{DT}/Y_{DD}	%	0.28	1.09	1.26	1.45	1.46	1.51
Y_{DT}/Y_{DD} (LASNEX)	%	0.30	1.70	1.62	...	1.24	1.29
$T_{i,DD}$	keV	4.2	2.7	2.7	3.7	3.6	3.8
$T_{i,DD}$ (LASNEX)	keV	3.7	3.0	2.8	...	3.6	3.8
T_e	keV	4.3	3.1	3.1	4.1	3.9	4.3
Bangtime (x ray)	ns	7.48	7.75	8.00	7.39	7.58	7.65
Bangtime (LASNEX)	ns	7.46	7.74	7.93	...	7.62	7.68
x-ray burnwidth	ns	0.28	0.29	0.26	0.30	0.25	0.28

initial 26-T B-field, we observed 2.9× yield increase and 1.1-keV temperature increase, with the inferred compressed B-field in the hot-spot estimated to be 7.1 ± 1.8 kT using measured primary DD-n and secondary DT-n neutron yields.

ACKNOWLEDGMENTS

This work was performed under the auspices of the U.S. Department of Energy by Lawrence Livermore National Laboratory under Contract No. DE-AC52-07NA27344 and by the LLNL-LDRD program under Project No. 20-SI-002. We gratefully acknowledge GA Contract No. 89233119CNA000063, the LLNL target fabrication and target diagnostics teams, as well as the operation teams for the execution of these experiments on OMEGA and the NIF.

AUTHOR DECLARATIONS

Conflict of Interest

The authors have no conflicts to disclose.

Author Contributions

Hong Sio: Conceptualization (equal); Data curation (lead); Formal analysis (equal); Investigation (lead); Methodology (equal); Writing – original draft (lead); Writing – review & editing (lead). **Bernard Kozioziemski:** Investigation (equal); Methodology (equal); Resources (equal); Supervision (supporting). **Evan Carroll:** Formal analysis (equal); Resources (equal). **Jeremy Kroll:** Project administration (equal); Resources (equal); Supervision (equal). **Dexter Yanagisawa:** Investigation (equal); Methodology (equal); Resources (equal); Supervision (equal). **Justin R. Angus:** Formal analysis (supporting); Investigation (supporting); Methodology (supporting). **Benjamin Bachmann:** Formal analysis (equal); Investigation (supporting); Methodology (supporting). **Alexander A. Baker:** Investigation (supporting); Methodology (supporting). **Leonardus Bimo Bayu Aji:** Investigation (supporting); Methodology (supporting). **S. D. Bhandarkar:** Investigation (supporting); Methodology (supporting); Project administration (supporting); Supervision (supporting). **Jeff Bude:** Funding acquisition (supporting); Resources (supporting). **John Douglas Moody:** Conceptualization (lead); Funding acquisition (lead); Investigation (equal); Project administration (lead); Resources (lead); Supervision (lead); Writing – review & editing (equal). **Laurent Divol:** Formal analysis (supporting); Investigation (supporting); Methodology (supporting). **Alison M. Engwall:** Investigation (supporting); Methodology (supporting). **Bryan Ferguson:** Investigation (supporting); Methodology (supporting); Validation (supporting). **Jon**

Fry: Investigation (supporting); Methodology (supporting); Project administration (supporting); Supervision (supporting). **Lisle Hagler:** Investigation (supporting); Methodology (supporting). **Edward Paul Hartouni:** Data curation (equal); Formal analysis (equal); Investigation (supporting); Methodology (supporting). **Mark Herrmann:** Funding acquisition (supporting); Resources (supporting). **Warren Hsing:** Funding acquisition (supporting); Project administration (supporting); Resources (supporting). **Dean Marcu Holunga:** Investigation (supporting); Methodology (supporting). **Jalal B. Javedani:** Investigation (supporting); Methodology (supporting). **Bradley Bolt Pollock:** Conceptualization (equal); Data curation (equal); Formal analysis (equal); Investigation (equal); Methodology (equal); Writing – review & editing (supporting). **Anthony Johnson:** Investigation (supporting); Methodology (supporting). **Shahab Firasat Khan:** Formal analysis (supporting); Investigation (supporting); Methodology (supporting); Software (supporting). **Daniel Kalantar:** Methodology (supporting); Resources (supporting). **T. Kohut:** Investigation (supporting); Supervision (supporting). **Burl G. Logan:** Investigation (supporting); Methodology (supporting). **Nathan Daniel Masters:** Investigation (supporting); Methodology (supporting). **Abbas Nikroo:** Investigation (supporting); Project administration (supporting); Supervision (supporting). **Nobuhiko Izumi:** Formal analysis (supporting); Investigation (supporting); Methodology (supporting). **Nicholas Orsi:** Investigation (supporting); Methodology (supporting). **Kenneth Piston:** Investigation (supporting); Methodology (supporting). **David J. Strozzi:** Conceptualization (equal); Data curation (equal); Formal analysis (equal); Investigation (equal); Methodology (supporting); Software (lead); Writing – review & editing (equal). **Christopher Provencher:** Methodology (supporting); Resources (supporting). **Arlen Rowe:** Methodology (supporting); Resources (supporting). **James D. Sater:** Investigation (supporting); Methodology (supporting). **Swanee J. Shin:** Investigation (supporting); Methodology (supporting). **Kenneth M. Skulina:** Project administration (supporting); Supervision (supporting). **William A. Stygar:** Investigation (supporting); Methodology (supporting). **Vincent Tang:** Funding acquisition (supporting); Project administration (supporting); Supervision (supporting). **Scott E. Winters:** Project administration (supporting); Supervision (supporting). **George Zimmerman:** Methodology (supporting); Software (supporting). **Jeremy P. Chittenden:** Investigation (supporting); Methodology (supporting); Supervision (equal). **Darwin D.-M Ho:** Conceptualization (supporting); Formal analysis (supporting); Investigation (supporting); Software (supporting); Validation (supporting). **Brian Daniel Appelbe:** Investigation (supporting); Methodology (supporting); Software (supporting). **Aidan Boxall:** Formal analysis (supporting); Investigation (supporting); Methodology (supporting). **Aidan Crilly:** Formal analysis (supporting); Investigation (supporting); Methodology (supporting). **Sam Thomas Jack O'Neill:** Formal analysis (supporting); Investigation (supporting); Methodology (supporting). **Daniel H. Barnak:** Formal analysis (supporting); Investigation (supporting); Methodology (supporting). **Jonathan R. Davies:** Investigation (supporting); Methodology (supporting); Supervision (supporting). **Jonathan Peebles:** Investigation (supporting); Methodology (supporting); Resources (supporting). **John Bae:** Investigation (supporting); Methodology (supporting). **Katrin Clark:** Investigation (supporting); Methodology (supporting). **Martin Havre:** Investigation (supporting); Methodology (supporting). **Christopher Alexander Walsh:** Formal analysis (equal); Investigation (equal); Methodology (equal); Software (equal); Validation (supporting); Writing – review & editing (supporting). **Michael Mauldin:** Investigation (supporting); Methodology (supporting). **M. Ratledge:** Investigation (supporting); Methodology (supporting). **Scott Vonhof:** Investigation (supporting); Methodology (supporting). **Patrick Adrian:** Formal analysis (supporting); Investigation (supporting); Methodology (supporting). **Benjamin L. Reichelt:** Investigation (supporting); Methodology (supporting). **Shinsuke Fujioka:** Investigation (supporting); Methodology (supporting). **Moshe Fraenkel:** Investigation (supporting); Resources (supporting). **Gregory Elijah Kemp:** Data curation (supporting); Formal analysis (equal). **Brandon Lahmann:** Formal analysis (equal); Methodology (equal); Validation (equal). **Sergei O. Kucheyev:** Conceptualization (equal); Investigation (equal); Methodology (equal); Project administration (supporting); Supervision (supporting); Writing – review & editing (supporting).

DATA AVAILABILITY

The data that support the findings of this study are available from the corresponding author upon reasonable request.

REFERENCES

[1] J. Lindl, "Development of the indirect-drive approach to inertial confinement fusion and the target physics basis for ignition and gain," Phys. Plasmas **2**, 3933 (1995).

[2] E. L. Dewald, M. Rosen, S. H. Glenzer, L. J. Suter, F. Girard, J. P. Jadaud, J. Schein, C. Constantin, F. Wagon, G. Huser, P. Neumayer, and O. L. Landen, "X-ray conversion efficiency of high-Z *hohlraum* wall materials for indirect drive ignition," Phys. Plasmas **15**, 072706 (2008).

[3] N. B. Meezan, L. J. Atherton, D. A. Callahan, E. L. Dewald, S. Dixit, E. G. Dzenitis, M. J. Edwards, C. A. Haynam, D. E. Hinkel, O. S. Jones, O. Landen, R. A. London, P. A. Michel, J. D. Moody, J. L. Milovich, M. B. Schneider, C. A. Thomas, R. P. J. Town, A. L. Warrick, S. V. Weber, K. Widmann, S. H. Glenzer, L. J. Suter, B. J. MacGowan, J. L. Kline, G. A. Kyrala, and A. Nikroo, "National Ignition Campaign *Hohlraum* energetics," Phys. Plasmas **17**, 056304 (2010).

[4] H. Abu-Shawareb and Indirect Drive ICF Collaboration, "Lawson criterion for ignition exceeded in an inertial fusion experiment," Phys. Rev. Lett. **129**, 075001 (2022).

[5] A. L. Kritcher, A. B. Zylstra, D. A. Callahan, O. A. Hurricane, C. R. Weber, D. S. Clark, C. V. Young, J. E. Ralph, D. T. Casey, A. Pak, O. L. Landen, B. Bachmann, K. L. Baker, L. Berzak Hopkins, S. D. Bhandarkar, J. Biener, R. M. Bionta, N. W. Birge, T. Braun, T. M. Briggs, P. M. Celliers, H. Chen, C. Choate, L. Divol, T. Döppner, D. Fittinghoff, M. J. Edwards, M. Gatu Johnson, N. Gharibyan, S. Haan, K. D. Hahn, E. Hartouni, D. E. Hinkel, D. D. Ho, M. Hohenberger, J. P. Holder, H. Huang, N. Izumi, J. Jeet, O. Jones, S. M. Kerr, S. F. Khan, H. Geppert Kleinrath, V. Geppert Kleinrath, C. Kong, K. M. Lamb, S. Le Pape, N. C. Lemos, J. D. Lindl, B. J. MacGowan, A. J. Mackinnon, A. G. MacPhee, E. V. Marley, K. Meaney, M. Millot, A. S. Moore, K. Newman, J.-M. G. Di Nicola, A. Nikroo, R. Nora, P. K. Patel, N. G. Rice, M. S. Rubery, J. Sater, D. J. Schlossberg, S. M. Sepke, K. Sequoia, S. J. Shin, M. Stadermann, S. Stoupin, D. J. Strozzi, C. A. Thomas, R. Tommasini, C. Trosseille, E. R. Tubman, P. L. Volegov, C. Wild, D. T. Woods, and S. T. Yang, "Design of an inertial fusion experiment exceeding the Lawson criterion for ignition," Phys. Rev. E **106**, 025201 (2022).

[6] A. B. Zylstra, A. L. Kritcher, O. A. Hurricane, D. A. Callahan, J. E. Ralph, D. T. Casey, A. Pak, O. L. Landen, B. Bachmann, K. L. Baker, L. Berzak Hopkins, S. D. Bhandarkar, J. Biener, R. M. Bionta, N. W. Birge, T. Braun, T. M. Briggs, P. M. Celliers, H. Chen, C. Choate, D. S. Clark, L. Divol, T. Döppner, D. Fittinghoff, M. J. Edwards, M. Gatu Johnson, N. Gharibyan, S. Haan, K. D. Hahn, E. Hartouni, D. E. Hinkel, D. D. Ho, M. Hohenberger, J. P. Holder, H. Huang, N. Izumi, J. Jeet, O. Jones, S. M. Kerr, S. F. Khan, H. Geppert Kleinrath, V. Geppert Kleinrath, C. Kong, K. M. Lamb, S. Le Pape, N. C. Lemos, J. D. Lindl, B. J. MacGowan, A. J. Mackinnon, A. G. MacPhee, E. V.

Marley, K. Meaney, M. Millot, A. S. Moore, K. Newman, J.-M. G. Di Nicola, A. Nikroo, R. Nora, P. K. Patel, N. G. Rice, M. S. Rubery, J. Sater, D. J. Schlossberg, S. M. Sepke, K. Sequoia, S. J. Shin, M. Stadermann, S. Stoupin, D. J. Strozzi, C. A. Thomas, R. Tommasini, C. Trosseille, E. R. Tubman, P. L. Volegov, C. R. Weber, C. Wild, D. T. Woods, S. T. Yang, and C. V. Young, "Experimental achievement and signatures of ignition at the National Ignition Facility," Phys. Rev. E **106**, 025202 (2022).

[7]E. I. Moses, J. Atherton, L. Lagin, D. Larson, C. Keane, B. MacGowan, R. Patterson, M. Spaeth, B. V. Wonterghem, P. Wegner, and R. Kauffman, "The National Ignition Facility: Transition to a user facility," J. Phys.: Conf. Ser. **688**, 012073 (2016).

[8]H. Abu-Shawareb and Indirect Drive ICF Collaboration, "Achievement of target gain, $G_{target} = 1.5$, in an inertial fusion experiment" (unpublished).

[9]G. A. Wurden, S. C. Hsu, T. P. Intrator, T. C. Grabowski, J. H. Degnan, M. Domonkos, P. J. Turchi, E. M. Campbell, D. B. Sinars, M. C. Herrmann, R. Betti, B. S. Bauer, I. R. Lindemuth, R. E. Siemon, R. L. Miller, M. Laberge, and M. Delage, "Magneto-inertial fusion," J. Fusion Energy **35**, 69–77 (2016).

[10]L. J. Perkins, D. D.-M. Ho, B. G. Logan, G. B. Zimmerman, M. A. Rhodes, D. J. Strozzi, D. T. Blackfield, and S. A. Hawkins, "The potential of imposed magnetic fields for enhancing ignition probability and fusion energy yield in indirect-drive inertial confinement fusion," Phys. Plasmas **24**, 062708 (2017).

[11]S. A. Slutz and R. A. Vesey, "High-gain magnetized inertial fusion," Phys. Rev. Lett. **108**, 025003 (2012).

[12]M. R. Gomez, S. A. Slutz, A. B. Sefkow, D. B. Sinars, K. D. Hahn, S. B. Hansen, E. C. Harding, P. F. Knapp, P. F. Schmit, C. A. Jennings, T. J. Awe, M. Geissel, D. C. Rovang, G. A. Chandler, G. W. Cooper, M. E. Cuneo, A. J. Harvey-Thompson, M. C. Herrmann, M. H. Hess, O. Johns, D. C. Lamppa, M. R. Martin, R. D. McBride, K. J. Peterson, J. L. Porter, G. K. Robertson, G. A. Rochau, C. L. Ruiz, M. E. Savage, I. C. Smith, W. A. Stygar, and R. A. Vesey, "Experimental demonstration of fusion-relevant conditions in magnetized liner inertial fusion," Phys. Rev. Lett. **113**, 155003 (2014).

[13]M. R. Gomez, S. A. Slutz, C. A. Jennings, D. J. Ampleford, M. R. Weis, C. E. Myers, D. A. Yager-Elorriaga, K. D. Hahn, S. B. Hansen, E. C. Harding, A. J. Harvey-Thompson, D. C. Lamppa, M. Mangan, P. F. Knapp, T. J. Awe, G. A. Chandler, G. W. Cooper, J. R. Fein, M. Geissel, M. E. Glinsky, W. E. Lewis, C. L. Ruiz, D. E. Ruiz, M. E. Savage, P. F. Schmit, I. C. Smith, J. D. Styron, J. L. Porter, B. Jones, T. R. Mattsson, K. J. Peterson, G. A. Rochau, and D. B. Sinars, "Performance scaling in magnetized liner inertial fusion experiments," Phys. Rev. Lett. **125**, 155002 (2020).

[14]P. Y. Chang, G. Fiksel, M. Hohenberger, J. P. Knauer, R. Betti, F. J. Marshall, D. D. Meyerhofer, F. H. Séguin, and R. D. Petrasso, "Fusion yield enhancement in magnetized laser-driven implosions," Phys. Rev. Lett. **107**, 035006 (2011).

[15]J. D. Moody, B. B. Pollock, H. Sio, D. J. Strozzi, D. D.-M. Ho, C. A. Walsh, G. E. Kemp, B. Lahmann, S. O. Kucheyev, B. Kozioziemski, E. G. Carroll, J. Kroll, D. K. Yanagisawa, J. Angus, B. Bachmann, S. D. Bhandarkar, J. D. Bude, L. Divol, B. Ferguson, J. Fry, L. Hagler, E. Hartouni, M. C. Herrmann, W. Hsing, D. M. Holunga, N. Izumi, J. Javedani, A. Johnson, S. Khan, D. Kalantar, T. Kohut, B. G. Logan, N. Masters, A. Nikroo, N. Orsi, K. Piston, C. Provencher, A. Rowe, J. Sater, K. Skulina, W. A. Stygar, V. Tang, S. E. Winters, G. Zimmerman, P. Adrian, J. P. Chittenden, B. Appelbe, A. Boxall, A. Crilly, S. O'Neill, J. Davies, J. Peebles, and S. Fujioka, "Increased ion temperature and neutron yield observed in magnetized indirectly driven D_2-filled capsule implosions on the National Ignition Facility," Phys. Rev. Lett. **129**, 195002 (2022).

[16]J. Soures, R. McCrory, T. Boehly, R. Craxton, S. Jacobs, J. Kelly, T. Kessler, J. Knauer, R. Kremens, S. Kumpan *et al.*, "OMEGA Upgrade laser for direct-drive target experiments," Laser Part. Beams **11**, 317–321 (1993).

[17]D. R. Lide, *CRC Handbook of Chemistry and Physics*84th ed. (CRC Press, 2003).

[18]J. D. Moody, A. Johnson, J. Javedani, E. Carroll, J. Fry, B. Kozioziemski, S. O. Kucheyev, B. G. Logan, B. B. Pollock, H. Sio, D. Strozzi, W. A. Stygar, V. Tang, and S. Winters, "Transient magnetic field diffusion considerations relevant to magnetically assisted indirect drive inertial confinement fusion," Phys. Plasmas **27**, 112711 (2020).

[19]L. B. B. Aji, A. M. Engwall, J. H. Bae, A. A. Baker, J. L. Beckham, S. J. Shin, X. L. Chavez, S. K. McCall, J. D. Moody, and S. O. Kucheyev, "Sputtered Au–Ta films with tunable electrical resistivity," J. Phys. D: Appl. Phys. **54**, 075303 (2020).

[20]L. B. Bayu Aji, A. M. Engwall, S. J. Shin, J. H. Bae, A. A. Baker, D. J. Strozzi, S. K. McCall, J. D. Moody, and S. O. Kucheyev, "Combinatorial sputter deposition of ultrathick Au-Bi alloy films," J. Phys. D: Appl. Phys. **55**, 485302 (2022).

[21]A. Engwall, L. Bayu Aji, A. Baker, S. Shin, J. Bae, S. McCall, J. Moody, and S. Kucheyev, "Effect of substrate tilt on sputter-deposited AuTa films," Appl. Surf. Sci. **547**, 149010 (2021).

[22]A. Engwall, L. Bayu Aji, S. Shin, A. Baker, J. Bae, S. McCall, J. Moody, and S. Kucheyev, "Sputter deposition of high electrical resistivity Au-Ta alloy coatings on rotating substrates," Thin Solid Films **758**, 139411 (2022).

[23]J. H. Bae, L. B. Bayu Aji, S. J. Shin, A. M. Engwall, M. H. Nielsen, A. A. Baker, S. K. McCall, J. D. Moody, and S. O. Kucheyev, "Gold-tantalum alloy films deposited by high-density-plasma magnetron sputtering," J. Appl. Phys. **130**, 165301 (2021).

[24]S. O. Kucheyev, S. J. Shin, L. B. Bayu Aji, J. H. Bae, A. M. Engwall, and G. V. Taylor, "Development of new magnetron sputter deposition processes for laser target fabrication," Fusion Sci. Technol. (published online).

[25]T. J. Orzechowski, M. D. Rosen, H. N. Kornblum, J. L. Porter, L. J. Suter, A. R. Thiessen, and R. J. Wallace, "The Rosseland mean opacity of a mixture of gold and gadolinium at high temperatures," Phys. Rev. Lett. **77**, 3545–3548 (1996).

[26]D. Colombant, M. Klapisch, and A. Bar-Shalom, "Increase in Rosseland mean opacity for inertial fusion hohlraum walls," Phys. Rev. E **57**, 3411–3416 (1998).

[27]J. Schein, O. Jones, M. Rosen, E. Dewald, S. Glenzer, J. Gunther, B. Hammel, O. Landen, L. Suter, and R. Wallace, "Demonstration of enhanced radiation drive in hohlraums made from a mixture of high-Z Wall materials," Phys. Rev. Lett. **98**, 175003 (2007).

[28]O. S. Jones, J. Schein, M. D. Rosen, L. J. Suter, R. J. Wallace, E. L. Dewald, S. H. Glenzer, K. M. Campbell, J. Gunther, B. A. Hammel, O. L. Landen, C. M. Sorce, R. E. Olson, G. A. Rochau, H. L. Wilkens, J. L. Kaae, J. D. Kilkenny, A. Nikroo, and S. P. Regan, "Proof of principle experiments that demonstrate utility of cocktail hohlraums for indirect drive ignition," Phys. Plasmas **14**, 056311 (2007).

[29]M. A. Barrios, J. D. Moody, L. J. Suter, M. Sherlock, H. Chen, W. Farmer, J. Jaquez, O. Jones, R. L. Kauffman, J. D. Kilkenny, J. Kroll, O. L. Landen, D. A. Liedahl, S. A. Maclaren, N. B. Meezan, A. Nikroo, M. B. Schneider, D. B. Thorn, K. Widmann, and G. Pérez-Callejo, "Developing an experimental basis for understanding transport in NIF hohlraum plasmas," Phys. Rev. Lett. **121**, 095002 (2018).

[30]H. N. Kornblum, R. L. Kauffman, and J. A. Smith, "Measurement of 0.1–3-keV x rays from laser plasmas," Rev. Sci. Instrum. **57**, 2179–2181 (1986).

[31]K. M. Campbell, F. A. Weber, E. L. Dewald, S. H. Glenzer, O. L. Landen, R. E. Turner, and P. A. Waide, "Omega Dante soft x-ray power diagnostic component calibration at the National Synchrotron Light Source," Rev. Sci. Instrum. **75**, 3768–3771 (2004).

[32]G. E. Kemp, M. S. Rubery, C. D. Harris, M. J. May, K. Widmann, R. F. Heeter, S. B. Libby, M. B. Schneider, and B. E. Blue, "A genetic algorithm approach for reconstructing spectral content from filtered x-ray diode array spectrometers," Rev. Sci. Instrum. **91**, 083507 (2020).

[33]D. T. Casey, C. A. Thomas, K. L. Baker, B. K. Spears, M. Hohenberger, S. F. Khan, R. C. Nora, C. R. Weber, D. T. Woods, O. A. Hurricane, D. A. Callahan, R. L. Berger, J. L. Milovich, P. K. Patel, T. Ma, A. Pak, L. R. Benedetti, M. Millot, C. Jarrott, O. L. Landen, R. M. Bionta, B. J. MacGowan, D. J. Strozzi, M. Stadermann, J. Biener, A. Nikroo, C. S. Goyon, N. Izumi, S. R. Nagel, B. Bachmann, P. L. Volegov, D. N. Fittinghoff, G. P. Grim, C. B. Yeamans, M. Gatu Johnson, J. A. Frenje, N. Rice, C. Kong, J. Crippen, J. Jaquez, K. Kangas, and C. Wild, "The high velocity, high adiabat, 'Bigfoot' campaign and tests of indirect-drive implosion scaling," Phys. Plasmas **25**, 056308 (2018).

[34]K. L. Baker, C. A. Thomas, D. T. Casey, S. Khan, B. K. Spears, R. Nora, T. Woods, J. L. Milovich, R. L. Berger, D. Strozzi, D. Clark, M. Hohenberger, O. A. Hurricane, D. A. Callahan, O. L. Landen, B. Bachmann, R. Benedetti, R. Bionta, P. M. Celliers, D. Fittinghoff, C. Goyon, G. Grim, R. Hatarik, N. Izumi, M. Gatu Johnson, G. Kyrala, T. Ma, M. Millot, S. R. Nagel, A. Pak, P. K. Patel, D. Turnbull, P. L. Volegov, and C. Yeamans, "High-performance indirect-drive cryogenic implosions at high adiabat on the National Ignition Facility," Phys. Rev. Lett. **121**, 135001 (2018).

[35]C. A. Thomas, E. M. Campbell, K. L. Baker, D. T. Casey, M. Hohenberger, A. L. Kritcher, B. K. Spears, S. F. Khan, R. Nora, D. T. Woods, J. L. Milovich, R. L. Berger, D. Strozzi, D. D. Ho, D. Clark, B. Bachmann, L. R. Benedetti, R. Bionta,

P. M. Celliers, D. N. Fittinghoff, G. Grim, R. Hatarik, N. Izumi, G. Kyrala, T. Ma, M. Millot, S. R. Nagel, P. K. Patel, C. Yeamans, A. Nikroo, M. Tabak, M. G. Johnson, P. L. Volegov, and S. M. Finnegan, "Experiments to explore the influence of pulse shaping at the National Ignition Facility," Phys. Plasmas **27**, 112708 (2020).
[36]E. L. Dewald, K. M. Campbell, R. E. Turner, J. P. Holder, O. L. Landen, S. H. Glenzer, R. L. Kauffman, L. J. Suter, M. Landon, M. Rhodes, and D. Lee, "Dante soft x-ray power diagnostic for National Ignition Facility," Rev. Sci. Instrum. **75**, 3759–3761 (2004).
[37]J. D. Moody, P. Datte, K. Krauter, E. Bond, P. A. Michel, S. H. Glenzer, L. Divol, C. Niemann, L. Suter, N. Meezan, B. J. MacGowan, R. Hibbard, R. London, J. Kilkenny, R. Wallace, J. L. Kline, K. Knittel, G. Frieders, B. Golick, G. Ross, K. Widmann, J. Jackson, S. Vernon, and T. Clancy, "Backscatter measurements for NIF ignition targets (invited)," Rev. Sci. Instrum. **81**, 10D921 (2010).
[38]G. B. Zimmerman and W. L. Kruer, "Numerical simulation of laser-initiated fusion," Comments Plasma Phys Controlled Fusion **2**, 51–60 (1975) see, https://www.osti.gov/etdeweb/biblio/7214660.
[39]J. A. Harte, W. E. Alley, D. S. Bailey, J. L. Eddleman, and G. B. Zimmerman, "LASNEX–A 2-D physics code for modeling ICF," Report No. UCRL-LR-105821-9-4 (1996).
[40]C. A. Walsh, S. O'Neill, J. P. Chittenden, A. J. Crilly, B. Appelbe, D. J. Strozzi, D. Ho, H. Sio, B. Pollock, L. Divol, E. Hartouni, M. Rosen, B. G. Logan, and J. D. Moody, "Magnetized ICF implosions: Scaling of temperature and yield enhancement," Phys. Plasmas **29**, 042701 (2022).
[41]J. P. Chittenden, S. V. Lebedev, C. A. Jennings, S. N. Bland, and A. Ciardi, "X-ray generation mechanisms in three-dimensional simulations of wire array Z-pinches," Plasma Phys. Controlled Fusion **46**, B457 (2004).
[42]A. Ciardi, S. V. Lebedev, A. Frank, E. G. Blackman, J. P. Chittenden, C. J. Jennings, D. J. Ampleford, S. N. Bland, S. C. Bott, J. Rapley, G. N. Hall, F. A. Suzuki-Vidal, A. Marocchino, T. Lery, and C. Stehle, "The evolution of magnetic tower jets in the laboratory," Phys. Plasmas **14**, 056501 (2007).
[43]L. Spitzer and R. Härm, "Transport phenomena in a completely ionized gas," Phys. Rev. **89**, 977–981 (1953).
[44]R. A. Lerche, V. Y. Glebov, M. J. Moran, J. M. McNaney, J. D. Kilkenny, M. J. Eckart, R. A. Zacharias, J. J. Haslam, T. J. Clancy, M. F. Yeoman, D. P. Warwas, T. C. Sangster, C. Stoeckl, J. P. Knauer, and C. J. Horsfield, "National Ignition Facility neutron time-of-flight measurements (invited)," Rev. Sci. Instrum. **81**, 10D319 (2010).
[45]T. J. Murphy, "The effect of turbulent kinetic energy on inferred ion temperature from neutron spectra," Phys. Plasmas **21**, 072701 (2014).
[46]R. E. Chrien, N. M. Hoffman, J. D. Colvin, C. J. Keane, O. L. Landen, and B. A. Hammel, "Fusion neutrons from the gas–pusher interface in deuterated-shell inertial confinement fusion implosions," Phys. Plasmas **5**, 768–774 (1998).
[47]B. Bachmann, T. Hilsabeck, J. Field, N. Masters, C. Reed, T. Pardini, J. R. Rygg, N. Alexander, L. R. Benedetti, T. Döppner, A. Forsman, N. Izumi, S. LePape, T. Ma, A. G. MacPhee, S. Nagel, P. Patel, B. Spears, and O. L. Landen, "Resolving hot spot microstructure using x-ray penumbral imaging (invited)," Rev. Sci. Instrum. **87**, 11E201 (2016).
[48]L. C. Jarrott, B. Bachmann, T. Ma, L. R. Benedetti, F. E. Field, E. P. Hartouni, R. Hatarik, N. Izumi, S. F. Khan, O. L. Landen, S. R. Nagel, R. Nora, A. Pak, J. L. Peterson, M. B. Schneider, P. T. Springer, and P. K. Patel, "Thermal temperature measurements of inertial fusion implosions," Phys. Rev. Lett. **121**, 085001 (2018).
[49]B. Bachmann, J. E. Ralph, A. B. Zylstra, S. A. MacLaren, T. Döppner, D. O. Gericke, G. W. Collins, O. A. Hurricane, T. Ma, J. R. Rygg, H. A. Scott, S. A. Yi, and P. K. Patel, "Localized mix-induced radiative cooling in a capsule implosion at the National Ignition Facility," Phys. Rev. E **101**, 033205 (2020).
[50]S. Atzeni and J. Meyer-Ter-Vehn, The Physics of Inertial Fusion: Beam Plasma Interaction, Hydrodynamics, Hot Dense Matter, *International Series of Monographs on Physics* (Oxford University Press, 2004).
[51]M. D. Cable and S. P. Hatchett, "Neutron spectra from inertial confinement fusion targets for measurement of fuel areal density and charged particle stopping powers," J. Appl. Phys. **62**, 2233–2236 (1987).
[52]H. G. Rinderknecht, M. J. Rosenberg, A. B. Zylstra, B. Lahmann, F. H. Séguin, J. A. Frenje, C. K. Li, M. Gatu Johnson, R. D. Petrasso, L. F. Berzak Hopkins, J. A. Caggiano, L. Divol, E. P. Hartouni, R. Hatarik, S. P. Hatchett, S. Le Pape, A. J. Mackinnon, J. M. McNaney, N. B. Meezan, M. J. Moran, P. A. Bradley, J. L. Kline, N. S. Krasheninnikova, G. A. Kyrala, T. J. Murphy, M. J. Schmitt, I. L. Tregillis, S. H. Batha, J. P. Knauer, and J. D. Kilkenny, "Using multiple secondary fusion products to evaluate fuel rhoR, electron temperature, and mix in deuterium-filled implosions at the NIF," Phys. Plasmas **22**, 082709 (2015).
[53]P. F. Schmit, P. F. Knapp, S. B. Hansen, M. R. Gomez, K. D. Hahn, D. B. Sinars, K. J. Peterson, S. A. Slutz, A. B. Sefkow, T. J. Awe, E. Harding, C. A. Jennings, G. A. Chandler, G. W. Cooper, M. E. Cuneo, M. Geissel, A. J. Harvey-Thompson, M. C. Herrmann, M. H. Hess, O. Johns, D. C. Lamppa, M. R. Martin, R. D. McBride, J. L. Porter, G. K. Robertson, G. A. Rochau, D. C. Rovang, C. L. Ruiz, M. E. Savage, I. C. Smith, W. A. Stygar, and R. A. Vesey, "Understanding fuel magnetization and mix using secondary nuclear reactions in magneto-inertial fusion," Phys. Rev. Lett. **113**, 155004 (2014).
[54]P. F. Knapp, P. F. Schmit, S. B. Hansen, M. R. Gomez, K. D. Hahn, D. B. Sinars, K. J. Peterson, S. A. Slutz, A. B. Sefkow, T. J. Awe, E. Harding, C. A. Jennings, M. P. Desjarlais, G. A. Chandler, G. W. Cooper, M. E. Cuneo, M. Geissel, A. J. Harvey-Thompson, J. L. Porter, G. A. Rochau, D. C. Rovang, C. L. Ruiz, M. E. Savage, I. C. Smith, W. A. Stygar, and M. C. Herrmann, "Effects of magnetization on fusion product trapping and secondary neutron spectra," Phys. Plasmas **22**, 056312 (2015).
[55]H. Sio, J. D. Moody, D. D. Ho, B. B. Pollock, C. A. Walsh, B. Lahmann, D. J. Strozzi, G. E. Kemp, W. W. Hsing, A. Crilly, J. P. Chittenden, and B. Appelbe, "Diagnosing plasma magnetization in inertial confinement fusion implosions using secondary deuterium-tritium reactions," Rev. Sci. Instrum. **92**, 043543 (2021).
[56]D. D. Ho, G. B. Zimmerman, A. L. Velikovich, R. M. Kulsrud, J. D. Moody, J. Harte, and A. L. Kritcher, "Magnetized ICF: Role of e-thermal conductivity on imploding shock and high-yield capsule designs," in *63rd Annual Meeting of the APS Division of Plasma Physics* (APS, 2021).
[57]C. A. Walsh, "Magnetized ablative Rayleigh-Taylor instability in three dimensions," Phys. Rev. E **105**, 025206 (2022).